The differing impact of air stagnation on summer ozone across Europe

Jose M. Garrido-Perez[1,2], Carlos Ordóñez[1], Ricardo García-Herrera[1,2] and Jordan L. Schnell[3]

[1]Dpto. Física de la Tierra y Astrofísica, Universidad Complutense de Madrid, Madrid, Spain.

[2]Instituto de Geociencias, CSIC-UCM, Madrid, Spain

[3]Department of Earth and Planetary Sciences, Northwestern University, Evanston, IL 60208, USA.

Corresponding author: Jose M. Garrido-Perez (josgarri@ucm.es)

Keywords: Air quality, air pollution, ozone, stagnation, meteorology

Abstract

We have examined the joint impact of daily maximum temperature and air stagnation on observed maximum daily 8-h running average (MDA8) and hourly near-surface ozone (O_3) over eight regions of Europe for the summer period 1998–2015. The percentage of stagnant area in a region is a better predictor of summer MDA8 O_3 in central/southern Europe (correlation coefficient R=0.50–0.70) than in the north (R=0.06–0.39). The correlations of MDA8 O_3 with temperature are higher than with stagnation for most regions, and the impact of stagnation on those correlations is region-dependent. MDA8 O_3 mixing ratios consistently increase over central/southern Europe under stagnant conditions, but this has not been found for some temperature ranges in the north. Under non-stagnant situations and relatively high temperatures (20–25 °C), southerly advection often brings aged air masses from more polluted areas to the receptor regions in the north. Furthermore, the occurrence of stagnation tends to amplify the ozone diurnal cycles in the center/south of the continent, yielding lower nighttime and higher daytime mixing ratios than on non-stagnant days, again with a less clear effect in the north. Changes in planetary boundary layer height, accumulation of ozone and precursors, and subsequent photochemical production during stagnant days are the presumed underlying mechanisms for the amplification of the diurnal cycles. The results from this study prove that the effects of stagnation on summer ozone are regionally dependent across Europe. Consequently, climate model projections of increases in stagnation should not directly be translated into degraded air quality without a proper assessment of the regional impacts.

1. Introduction

Tropospheric ozone (O_3) is one of the main pollutants linked to health and environmental impacts (Ashmore, 2005; REVIHAAP, 2013; Tai et al., 2014). It is transported from the stratosphere, and produced by photochemical reactions between primary precursors such as nitrogen oxides (NO_x) and volatile organic compounds (VOCs). Observational studies have shown strong relationships of O_3 with meteorological parameters. Understanding such relationships is often complicated by the covariance of the meteorological variables as well as by the effect of short- and long-term emission changes. Ambient air temperature is the most correlated variable with daily ozone maxima in summer (Bloomfield et al., 1996; Xu et al., 1996; Kuebler et al., 2001; Tarasova and Karpetchko, 2003; Ordóñez et al., 2005). The relationship between both variables is driven by several well-known temperature-dependent mechanisms: the thermal decomposition of the NO_x reservoir species peroxyacetyl nitrate (PAN, $CH_3COO_2NO_2$) (Orlando et al., 1992), the temperature-dependent emissions of both VOCs from vegetation and NO_x from soil (Fehsenfeld et al., 1992; Simpson, 1995), the extra evaporation of anthropogenic VOCs at high temperatures (Vautard et al., 2005), or the high stomatal resistance at elevated temperatures, which limits the dry deposition of ozone to vegetation (Wesely, 1989). Nevertheless, the temperature – O_3 relationship is complex and can only partially be explained by the mentioned processes. As an example, Porter and Heald (2019) have estimated that the covariance of temperature with other meteorological variables explains over 40% of the ozone-temperature correlation in the United States (US) and up to 60% in Europe. There are a number of relevant non-temperature meteorological processes that may contribute to this covariance. Among others, air stagnation is a potential candidate as it is characterized by stable weather conditions with poor ventilation, leading to the accumulation of pollutants close to the surface (Jacob and Winner, 2009; Dawson et al., 2014; Fiore et al., 2015).

Enhanced ozone concentrations under stagnant conditions have been documented for the US (Leibensperger et al., 2008; Schnell and Prather, 2017) and Europe (Garrido-Perez et al., 2018). The relationship between a simplified air stagnation index (ASI) defined by Horton et al. (2012) – based on absolute thresholds of daily precipitation, 10 m and 500 hPa wind speed –, temperature and O_3 has been closely examined by some studies for the US. Sun et al. (2017) found that the probability of high O_3 days increases with the co-occurrence of high temperature and stagnation, and that the occurrence of successive stagnation days further enhances this likelihood. Schnell and Prather (2017) showed that air stagnation and extreme levels of O_3 and temperature tend to co-occur in large-scale, multiday and coherent structures. In Europe, Garrido-Perez et al. (2018) reported significant changes in the frequency distribution of O_3 when stagnation occurs as well as a strong build-up of the O_3 mixing ratios during widespread stagnant episodes. These evidences are in line with the hypothesis of Horton et al. (2012), who projected 21st century increases in stagnation frequency over several highly populated regions of the globe and suggested a potential to enhance the accumulation of near-surface ozone. However, the relationship between stagnation and summer ozone has been reported to be weak over some regions of the US (Kerr and Waugh, 2018). That study noted the limited skill of the ASI to explain air pollution events and indicated an erratic overlap between stagnation and pollutant extremes in the US, especially in the Northeast. Consequently, they advised against the use of this common index as a metric to examine pollution events and recommended testing new indices considering other meteorological predictors such as planetary boundary layer (PBL) height and temperature.

Building on the results by Kerr and Waugh (2018) for the US, the aims of this study are to (i) evaluate whether the ASI is an adequate index of summer ozone pollution over different regions of Europe and (ii) analyze the complementarity of this index with temperature to understand summer ozone variability in the continent. To do so, we firstly investigate the temporal co-variability of ozone, temperature and air stagnation. Then we evaluate whether the relationship between O_3 and temperature differs under stagnant and non-stagnant situations. Finally, we explore the diurnal cycle of O_3 in order to understand the response of this pollutant to stagnation and the mechanisms involved.

2. Data and methods

2.1. Ozone and meteorological data

We use interpolated datasets of observed maximum daily 8-h running average near-surface ozone (MDA8 O_3) and hourly ozone volume mixing ratios over Europe at 1.0° × 1.0° resolution for the 18 summers (JJA) during the period 1998 – 2015. The summer means of MDA8 O_3 from these datasets, excluding data over the Balkans (see below), are illustrated in Supplementary Figure S1. The data have been generated by merging non-traffic observations obtained from two databases – the European Environment Agency's air quality database (AirBase) and the European Monitoring and Evaluation Programme (EMEP) (Tørseth et al., 2012) – with the objective mapping algorithm developed by Schnell et al. (2014, 2015). These data have recently been used by several studies (Otero et al., 2016, 2018; Carro-Calvo et al. 2017; Ordóñez et al., 2017; Garrido-Perez et al., 2018) to understand the meteorological drivers of ozone in Europe. In particular, Carro-Calvo et al. (2017) applied the k-means clustering technique to obtain nine regions where O_3 shows coherent spatiotemporal patterns. The regions from that study will be used here to examine the relationship among air stagnation, temperature and O_3 in a consistent way. However, we have decided to exclude one of the regions (the Balkans) from our analysis because of inhomogeneities in the O_3 time series reported by that study. From west to east and from north to south, the regions analyzed here roughly cover the British Isles (BRIT), northern-central Europe (NCE), northern Scandinavia (NSC), the Baltic region (BALT), the Iberian Peninsula (IBE), western Europe (WE), southern-central Europe (SCE) and eastern Europe (EE). This regionalization is displayed on Figure 1.

We also use daily mean fields of sea level pressure (SLP); daily mean 10 m ($\widehat{U}_{10m}$), 850 hPa ($\widehat{U}_{850hPa}$) and 500 hPa ($\widehat{U}_{500hPa}$) wind; daily accumulated precipitation (pr); daily maximum temperature (T_{max}), and PBL heights from the European Centre for Medium-Range Weather Forecasts (ECMWF) ERA-Interim reanalysis (Dee et al., 2011). We regridded the original 0.75° × 0.75° horizontal resolution data onto the 1.0° × 1.0° grid of O_3 using bilinear interpolation. $\widehat{U}_{10m}$, $\widehat{U}_{500hPa}$ and pr data are needed for the calculation of the ASI (see Section 2.2), while SLP and $\widehat{U}_{850hPa}$ are employed for the comparison of the atmospheric circulation patterns in the lower troposphere during stagnant and non-stagnant days. Daily averages of SLP and wind speed have been computed as the average of the four analysis values at 00, 06, 12 and 18 UTC for each day. pr has been calculated by summing the 12-h accumulated precipitation forecast at 00 and 12 UTC. T_{max} has been computed as the maximum from all the temperature values forecasted for each day, following the recommendations at https://confluence.ecmwf.int/pages/viewpage.action?pageId=58157862 (last access: 20 September 2019). The forecast values of PBL height have also been used at the standard

meteorological hours 00, 06, 12 and 18 UTC to better understand the diurnal cycles of O_3.

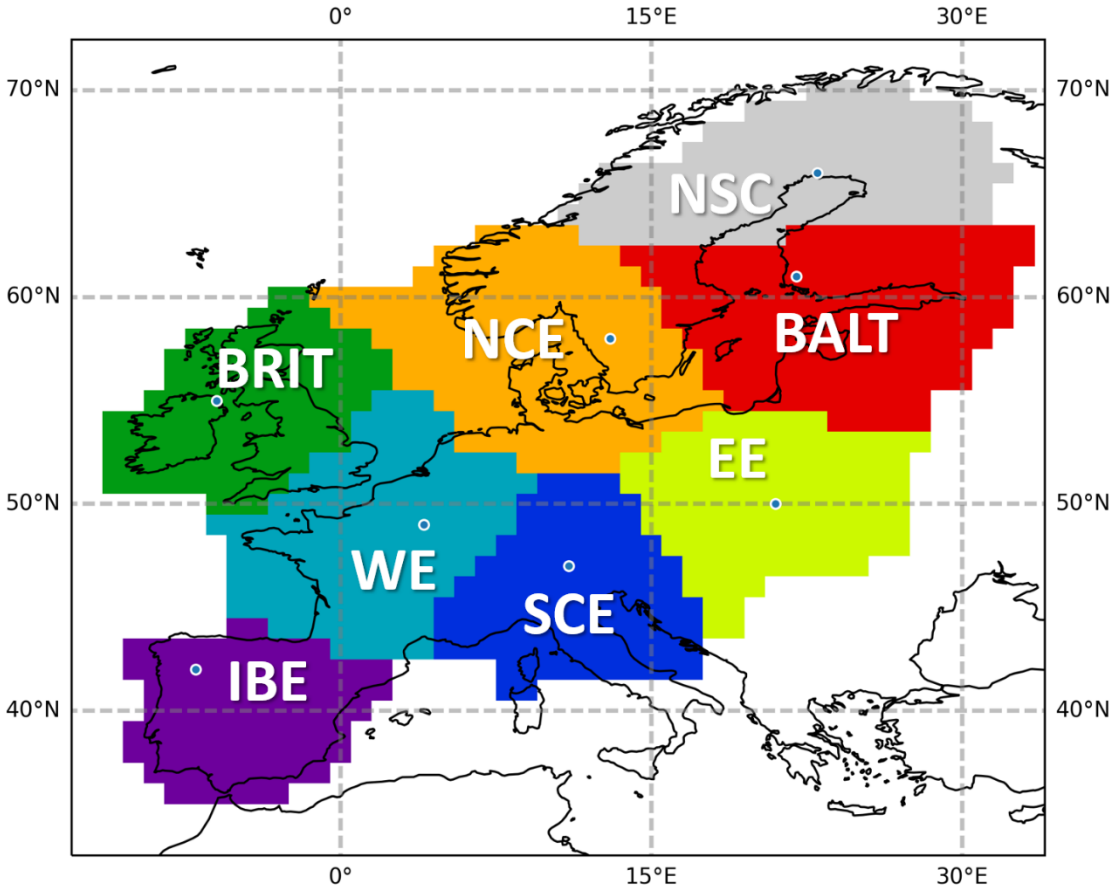

Figure 1. Regionalization of summer MDA8 O_3. From west to east and from north to south the regions roughly correspond to the British Isles (BRIT), northern-central Europe (NCE), northern Scandinavia (NSC), the Baltic region (BALT), the Iberian Peninsula (IBE), western Europe (WE), southern-central Europe (SCE) and eastern Europe (EE). Blue circles represent the land grid cells where the correlations between the standardized anomalies of the MDA8 O_3 time series and those of the respective centroid maximize (see details in the main text).

2.2. Methods

Air stagnation is characterized by meteorological conditions that impede the scavenging, horizontal dispersion and vertical escape of pollutants in the lower troposphere (Horton et al., 2012, and references therein). Different air stagnation indices have been proposed in the literature to identify the conditions conducive to air mass stagnation (see e.g. Garrido-Perez et al., 2018, and references therein). Such indices are usually defined by using predefined thresholds for daily average meteorological fields.

In this work we have used the simplified air stagnation index defined by Horton et al. (2012). This ASI is an adaptation of another index originally developed for the US that is currently being used by the US National Oceanic and Atmospheric Administration (NOAA) National Climatic Data Center (NCDC) (Wang and Angell, 1999). With the application of Horton's ASI, a reanalysis grid cell is considered as stagnant if three conditions are simultaneously met on a given day: $\widehat{U}_{10m}$ < 3.2 m s^{-1}, $\widehat{U}_{500hPa}$< 13.0 m s^{-1} and pr < 1 mm. This results in a high frequency of stagnation in some parts of

Mediterranean Europe (around 40% of the days), moderate frequency in central Europe and Scandinavia (~25% of the days) and low over the British Isles (~15% of the days) during the summer months of 1998–2015 (see Figure S2).

The index has recently been used to characterize the spatiotemporal variability and impact of air stagnation on air quality in Europe (Garrido-Perez et al., 2018), but the relationship between stagnation and summer ozone over different parts of the continent might be sensitive to the ASI component threshold definition. To account for this, we have repeated some of the analyses presented here by varying the three thresholds from 25 to 175% of their standard values. Overall, we have found relatively small changes both in the ozone–stagnation correlations (Table 1) and the ozone dependence on stagnation (Figure 3) in all regions when the three thresholds are within 75–125% of their standard values (not shown). This indicates that the results presented in this study are not very sensitive to the precise definition of stagnant conditions, as previously found by Kerr and Waugh (2018) for the US. Finally, we would also like to note that more complex air stagnation indices have recently been developed but they are specifically adapted to particulate matter (e.g. Wang et al., 2016, 2018; Huang et al., 2018).

3. Relationship between MDA8 O_3, temperature and stagnation

Table 1 shows the Pearson correlation coefficients (R) between the daily time series of average T_{max}, average MDA8 O_3 and the percentage of the area under stagnant conditions for each region in summer. The significance of these correlations has been determined through two-tailed t-tests as indicated in von Storch and Zwiers (1999), taking into account that the data exhibit serial correlation, i.e. the daily values of these variables are not independent of their own future and past values because of the effect of the meteorological persistence (see e.g. Wilks, 2011). This implies that the effective number of degrees of freedom (ν_{eff}) is lower than that directly determined from the sample size, increasing the p-value of the test and reducing the level of statistical significance. Accordingly, we have calculated ν_{eff} following Eq. 1 of Hu et al. (2017) before assessing significance. This way, the three fields significantly correlate at the 95% confidence level for all regions, with the exception of the stagnation – MDA8 O_3 correlation in NSC. However, there is considerable spatial heterogeneity across Europe, with higher correlations in the central/southern clusters (IBE, WE, SCE and EE) than in the northern clusters (BRIT, NCE, NSC and BALT). The correlations are above 0.5 over the central/southern regions, with the exception of T_{max} – MDA8 O_3 in IBE and T_{max} – stagnation in EE, while they tend to be well below that value for the northern regions. As expected, the correlations of MDA8 O_3 with T_{max} are higher than with the percentage of stagnant area for most regions, although the latter can be considered as a good predictor of ozone in central/southern Europe. On the other hand, T_{max} and stagnation present high correlations in the southern clusters as well as in NCE, evidencing the strong covariability between both variables. Hence, it is unclear whether the high correlations between O_3 and stagnation in the southern regions reflect the ozone-temperature relationship or are due to other processes.

Table 1. Pearson product-moment correlation coefficients (R) between the daily time series of average T_{max}, average MDA8 O_3 and the percentage of stagnant area (AS) for each region during summer (JJA) 1998 – 2015. The geographical locations of the regions are displayed in Figure 1. All values are statistically significant at the 95% confidence level, except where noted by asterisk (*).

	BRIT	NCE	NSC	BALT	IBE	WE	SCE	EE
T_{max} – MDA8 O_3	0.18	0.52	0.35	0.48	0.42	0.70	0.77	0.73
AS – MDA8 O_3	0.24	0.39	0.06*	0.27	0.56	0.62	0.70	0.50
T_{max} - AS	0.23	0.47	0.24	0.33	0.51	0.53	0.58	0.44

To try to understand the influence of air stagnation in the T_{max} – MDA8 O_3 relationship, we have evaluated if this relationship changes with the occurrence of stagnation. For this purpose, we have first computed the correlation coefficients between the daily time series of T_{max} and MDA8 O_3 for each grid cell, considering stagnant and non-stagnant days separately (Figure 2). The spatial distribution of the correlations displayed in the figure is consistent with that shown in Table 1, as the highest values are generally found for WE, SCE and EE. Nevertheless, Figure 2 presents a complex picture of the effect of stagnation on the T_{max} – MDA8 O_3 relationship across Europe. On the one hand, stagnation seems to contribute to strengthening this relationship over large parts of the three regions that present high correlations. Regions characterized by relatively low ozone levels and stagnation frequency (e.g. the UK and NCE, see Figures S1 and S2) also present higher correlations when stagnation occurs. These results are in line with a previous study that has highlighted the contribution of stagnation to increasing the probability of occurrence of a high ozone day given a high-temperature day in the US (Sun et al., 2017). On the other hand, there are some parts of the south and east of the continent where these correlations do not increase with the occurrence of stagnation. The correlations even decrease over an area roughly covering the southeastern half of IBE, where stagnation is relatively common in summer (see Figure S2) and the day-to-day ozone variability – as measured by the relative standard deviation of summer MDA8 O_3 – is lower than in the rest of the continent (not shown).

From these results, no clear conclusions can be drawn on the contribution of stagnation to the ozone-temperature relationship. Actually, these correlations may depend on a number factors whose effects are difficult to disentangle. First, the range of variability of both daily temperature and ozone differs considerably across Europe. Second, the ozone-temperature relationship tends to be linear only within specific temperature ranges (e.g. Bloomer et al., 2009), high enough to favor photochemical production but below some high thresholds that may lead to ozone suppression at some locations (Steiner et al., 2010; Shen et al., 2016; Meehl. et al., 2018). Finally, the strengthening of the O_3–T_{max} correlations under stagnant conditions found for some regions might partly occur because elevated temperatures often coincide with stagnant days. Henceforth, to remove as much as possible the influence of the different factors that limit our understanding of the impact of stagnation on ozone, we will perform composite analyses within specific temperature bins separately for each region.

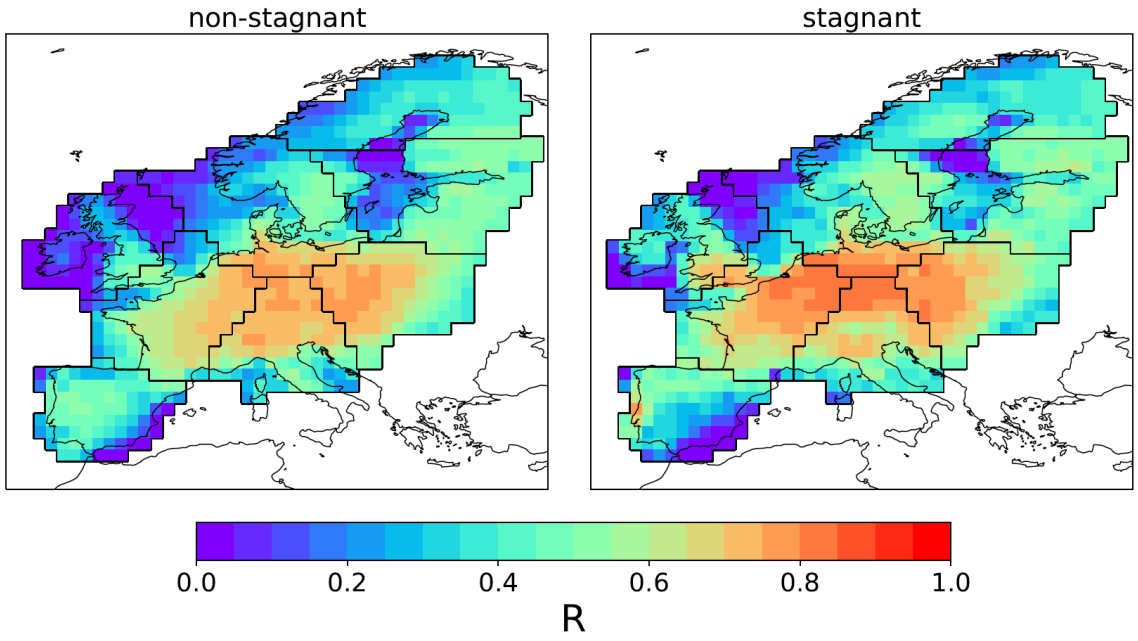

Figure 2. Pearson product-moment correlation coefficient (R) between the 1998 – 2015 summer (JJA) daily time series of T_{max} and MDA8 O_3 for days without (left) and with (right) stagnation in each grid cell.

Figure 3 shows boxplots of MDA8 O_3 within 3 °C temperature bins for days with (red) and without (blue) stagnation, considering every grid cell within each region. Overall, the relationship of ozone with temperature starts to be linear above ~16 °C, with coefficients of determination (R^2) above 0.93 for all regions. The ozone distributions under stagnant and non-stagnant conditions are significantly different at the 95% confidence level for most temperature bins and regions, as determined through the two-sample Kolmogorov-Smirnov test (e.g. Wilks, 2011) and indicated by starts on top of the pairs of boxes. In central/southern Europe, the presence of stagnant conditions causes consistently higher MDA8 O_3 regardless of the temperature bin (around 4–6 ppb on average considering the mean values of each bin), but this is not always the case for the northern regions. For instance, ozone is significantly reduced on stagnant days within 24–27 °C in BRIT or above ~21 °C in NSC, and there is a minor impact of stagnation on ozone within 21–30 °C in BALT. Furthermore, stagnation does not seem to exert a significant impact within 27–30 °C in that region and 24–27 °C in NCE.

To understand these results we have compared the typical circulation patterns in the lower troposphere for stagnant and non-stagnant days in all regions. As stagnant conditions in the reanalysis are determined on a grid cell by grid cell basis, we have first identified a representative location for each region and then produced composite maps of daily SLP and 850 hPa wind, considering stagnant and non-stagnant days at each location. For the selection of such locations we have looked for the land grid cells where the correlation between the daily time series of standardized anomalies of summer MDA8 O_3 and that of the respective centroid (i.e. time series of the average standardized anomalies within the cluster) maximize. The choice of standardized anomalies instead of absolute values of MDA8 O_3 is justified by the fact that the former were used for the identification of the regions used here (Carro-Calvo et al., 2017). The eight representative locations are displayed as circles in Figure 1. Then we have composited SLP and 850 hPa wind data for stagnant and non-stagnant days at each location with T_{max} within 20–25 °C. This temperature interval has been chosen because it is typical of fair weather conditions favorable for ozone production in northern Europe. Moreover, around 22–44% of the

summer days lay within this temperature range at 7 out of the 8 locations, with the exception of only ~3% of the days for the grid cell in BRIT. Consequently, this temperature interval also guarantees a representative enough number of occurrences to draw solid conclusions for most locations.

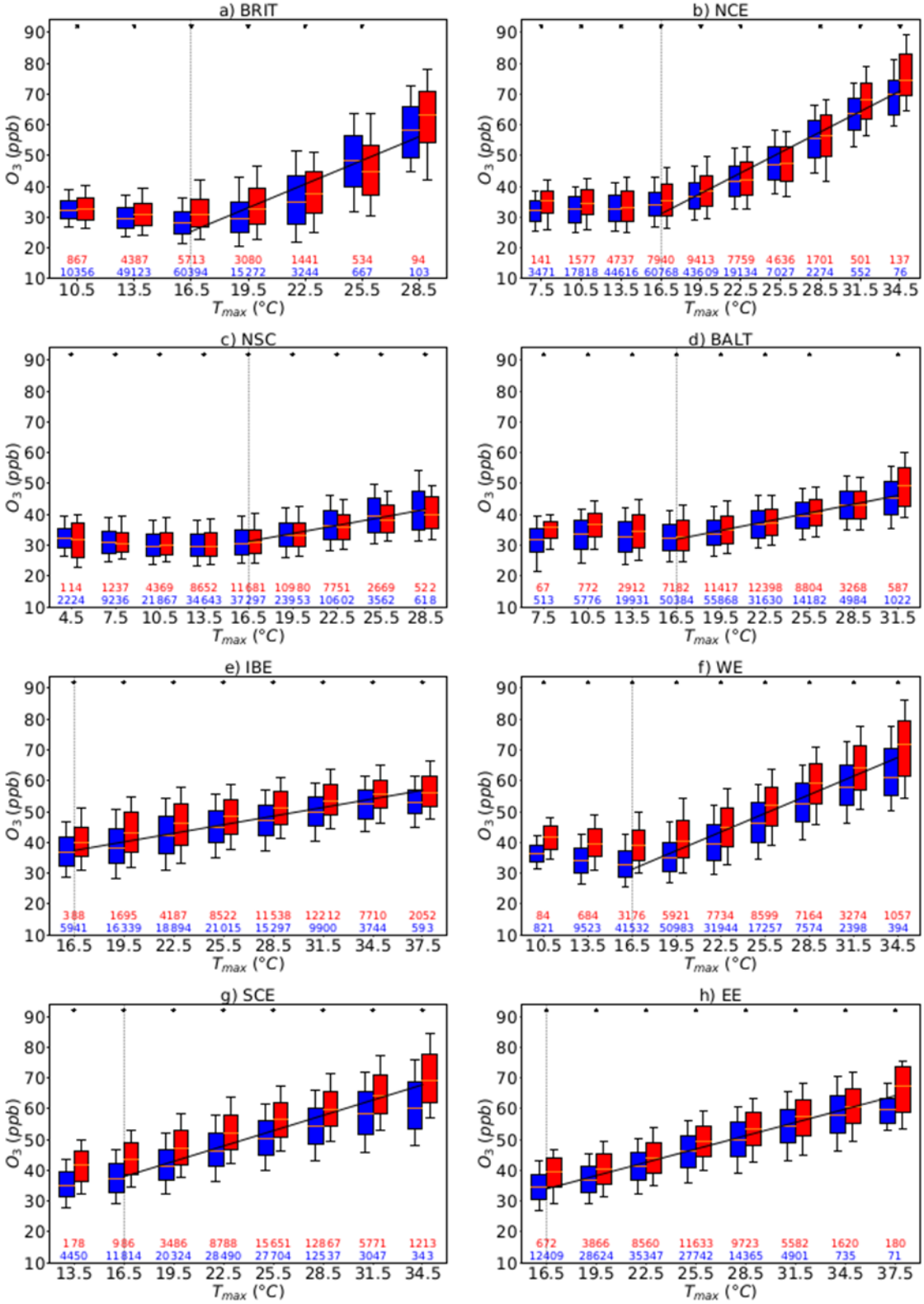

Figure 3. Boxplots of 1998 – 2015 summer MDA8 O_3 in 3 °C bins of T_{max}, considering all grid cells in each region. Blue (red) boxes represent days classified as non-stagnant (stagnant). The boxes extend from the lower (Q1) to the upper (Q3) quartile values of the data, with a horizontal line indicating the position of the median (Q2). The whiskers extend from the boxes to show the range of the data between the 10^{th} and 90^{th} percentiles. The x-axis tick labels represent the middle point for each temperature bin. Temperature bins are only shown if they include at least 50 cases (number of cases = number of days × number of sites) for both stagnant and non-stagnant conditions; as a result the range of temperatures shown on the x-axis varies with the region. The numbers of stagnant (red) and non-stagnant (blue) cases are indicated below the corresponding temperature bins. Black stars are shown over each pair of boxes if their MDA8 O_3 distributions are significantly different at the 95% confidence level (determined through the two-sample Kolmogorov-Smirnov test). The vertical dotted lines indicate the temperature bins with centers at 16.5°C. Linear regressions of the mean MDA8 O_3 within each temperature bin (considering both stagnant and non-stagnant cases) on T_{max} (mid-points of the intervals) have been drawn for the temperature bins ≥ 16.5°C.

Figures 4 and 5 respectively illustrate the circulation patterns on stagnant and non-stagnant days within the mentioned 20–25 °C temperature range in the northern locations (BRIT, NCE, NSC and BALT). As expected, air stagnation situations are characterized by anticyclonic circulation and weak wind in the lower troposphere over the affected regions (Figure 4). The composite for NCE during non-stagnant days (Figure 5b) displays westerly to southwesterly flow from the North Sea to the region. This situation enhances the transport of relatively clean marine air masses to the receptor region, resulting in ozone levels somewhat below those of stagnant days (Figure 3b). On the other hand, BRIT, NSC and BALT are under the effect of southerly advection during non-stagnant days (Figure 5, a, c, d) and, as shown above, do not display clear enhancements of MDA8 O_3 (Figure 3, a, c, d) despite the low wind speeds found on stagnant days (Figure 4, a, c, d). The results for these three regions are in line with the findings by Carro-Calvo et al. (2017), who reported that ozone extremes (exceedances of the summer 95^{th} percentile) in the north of the continent tend to be at least partly caused by the advection of polluted, warm air masses from central/southern regions. This is consistent with the strong meridional gradient of MDA8 O_3 in Europe (see Figure S1). In the receptor regions, wind speeds are relatively high under such situations, which means that high ozone days often concur with non-stagnant days. This explains the unclear impact of stagnation on MDA8 O_3 within some temperature bins in northern Europe. However, as anticipated before, the results for BRIT should be interpreted with caution because of the reduced data sample (only around 3% of the summer days with temperatures within 20–25 °C, less than one third of them with stagnation). In the case of central-southern Europe, stagnant days are associated with lower wind speeds than non-stagnant days for all regions, as well as with a suppression of westerly advection over WE and EE (see Figures S3 and S4).

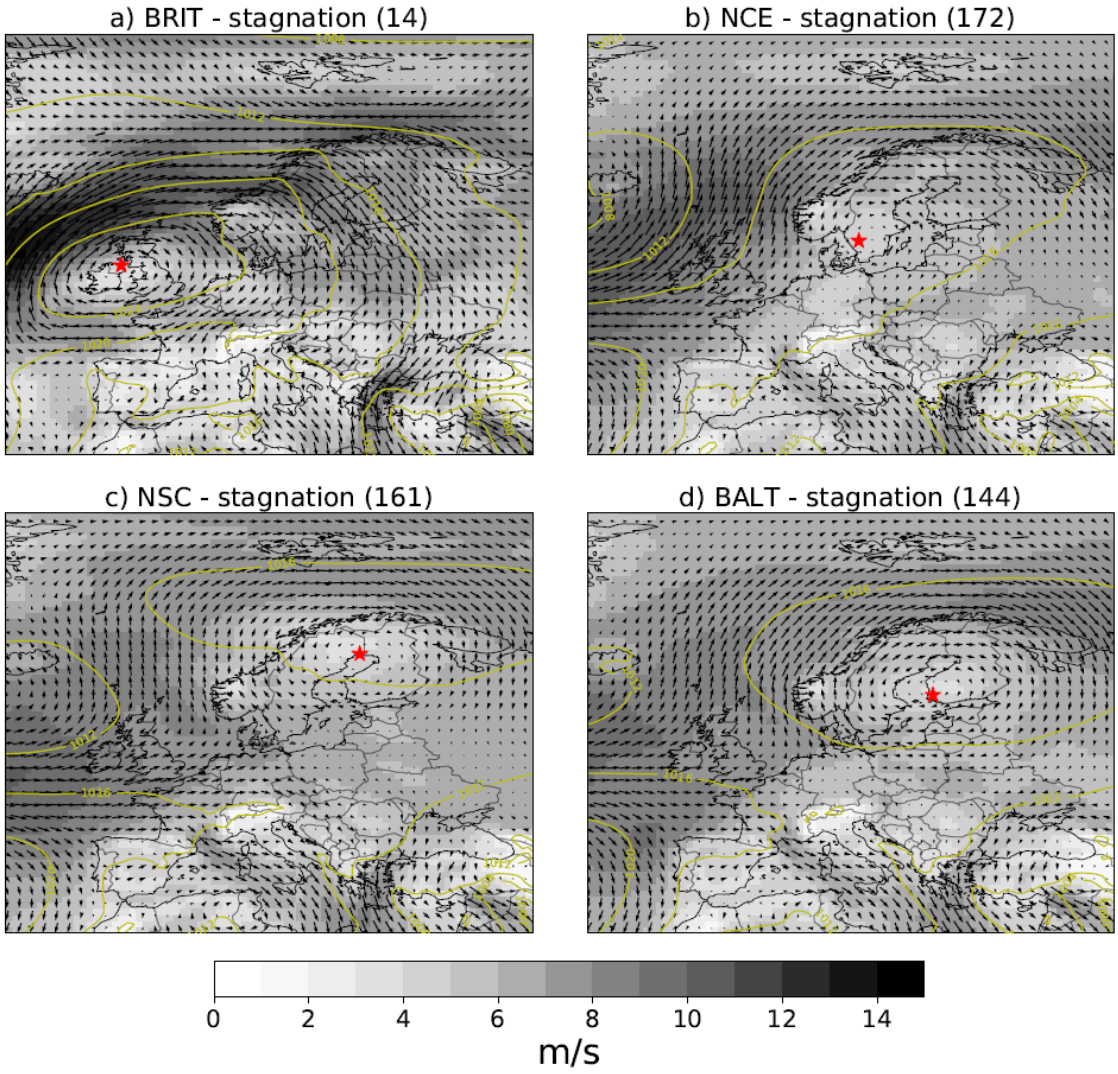

Figure 4. Composites of SLP and 850 hPa wind speed on days with stagnant conditions and T_{max} within 20 – 25 °C, at the representative locations (red stars) of BRIT, NCE, NSC and BALT, during the summer months from 1998 to 2015. The yellow contour lines, grey shading and arrows respectively represent SLP (hPa), and module and vectors of 850 hPa wind speed (m/s). The numbers in brackets represent the number of days considered in each composite.

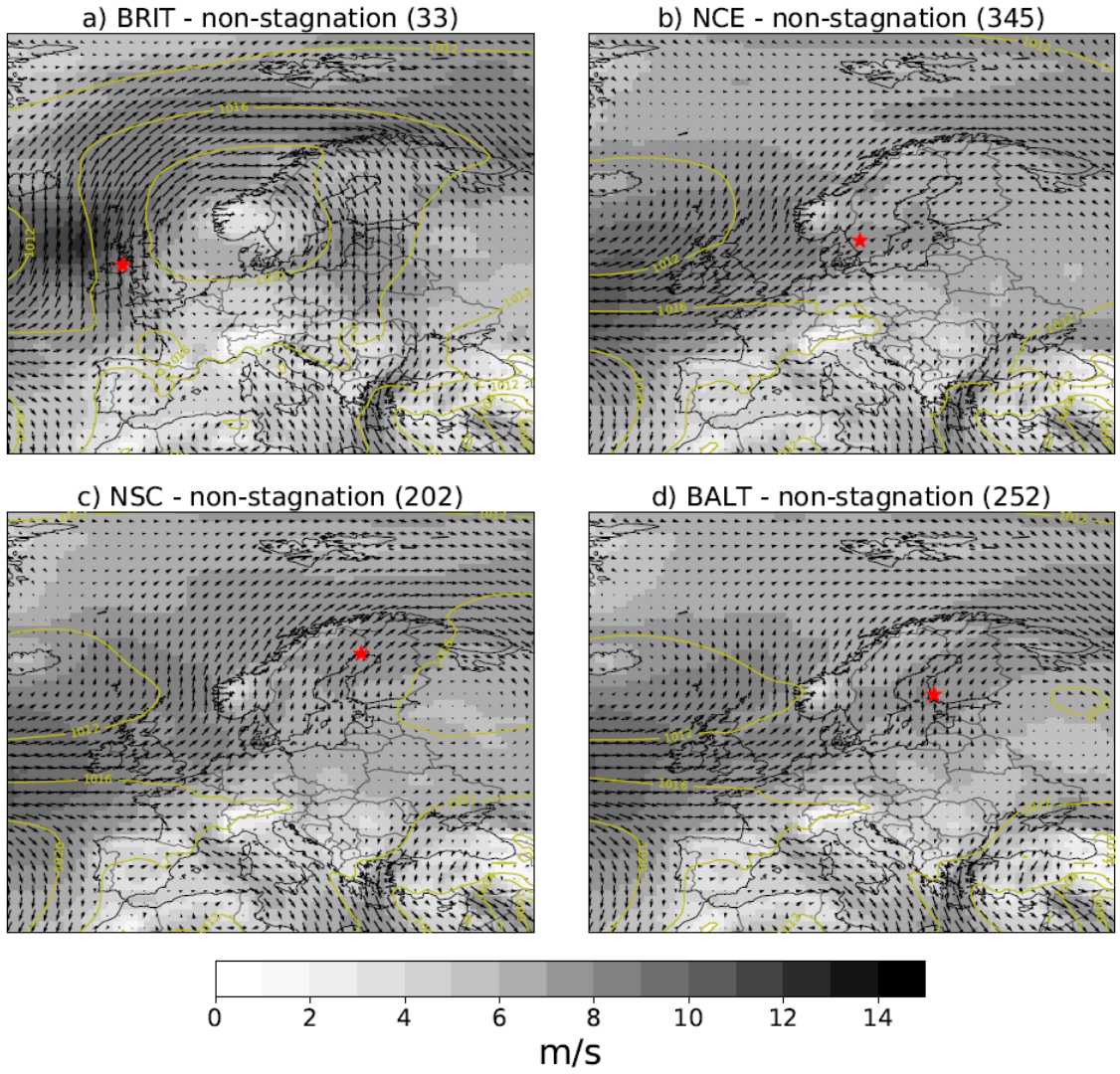

Figure 5. As Figure 4 but for non-stagnant days.

4. Impact of stagnation on the O_3 diurnal cycle

To better understand the ozone response to stagnation, we have compared the diurnal cycles of this pollutant in each region for stagnant and non-stagnant days. Our analyses are inspired by those of Pyrgou et al. (2018), who examined the effect of heatwave conditions on the diurnal cycle of ozone on a Mediterranean island. As in that study, the main limitation of our approach is that the evaluation of diurnal cycles is done based on average or accumulated values of meteorological variables (wind speed and precipitation in our particular case) during the whole day. We have also examined the impact of the persistence of stagnation on these diurnal cycles to investigate if the day-to-day evolution of ozone is affected by stagnation. As before, for the sake of simplicity, these analyses have been carried out for a single land grid cell in each cluster (blue circles in Figure 1) considering days with T_{max} within 20–25 °C. Results are reported here only for BALT and SCE as two representative regions of northern and central/southern Europe, respectively (Figure 6), and for the rest of clusters in the Supplementary Material (Figure S5 for the northern regions and Figure S6 for the central/southern regions).

It is well known that O_3 diurnal cycles are characterized by high concentrations during daylight hours and low values during the late night and early morning, as seen on the left and middle panels of Figures 6, S5 and S6. Both the entrainment of ozone-rich air from aloft during the development of the well-mixed PBL and photochemical production lead to the build-up of the ozone mixing ratios at daytime, with a daily maximum in the afternoon. On the other hand, O_3 mixing ratios decrease during the night because of the cease of production as well as the destruction by dry deposition to surfaces and titration by nitrogen monoxide (NO) in the shallow nocturnal PBL (e.g. Petetin et al., 2016, and references therein). The daily ozone minimum often occurs at a time with low PBL and elevated NO_x emissions from traffic during the morning rush hour. The amplitude of the diurnal cycle (defined as the difference between the maximum and the minimum hourly O_3 mixing ratios) is geographically dependent due to differences in the emission patterns and climates of each region.

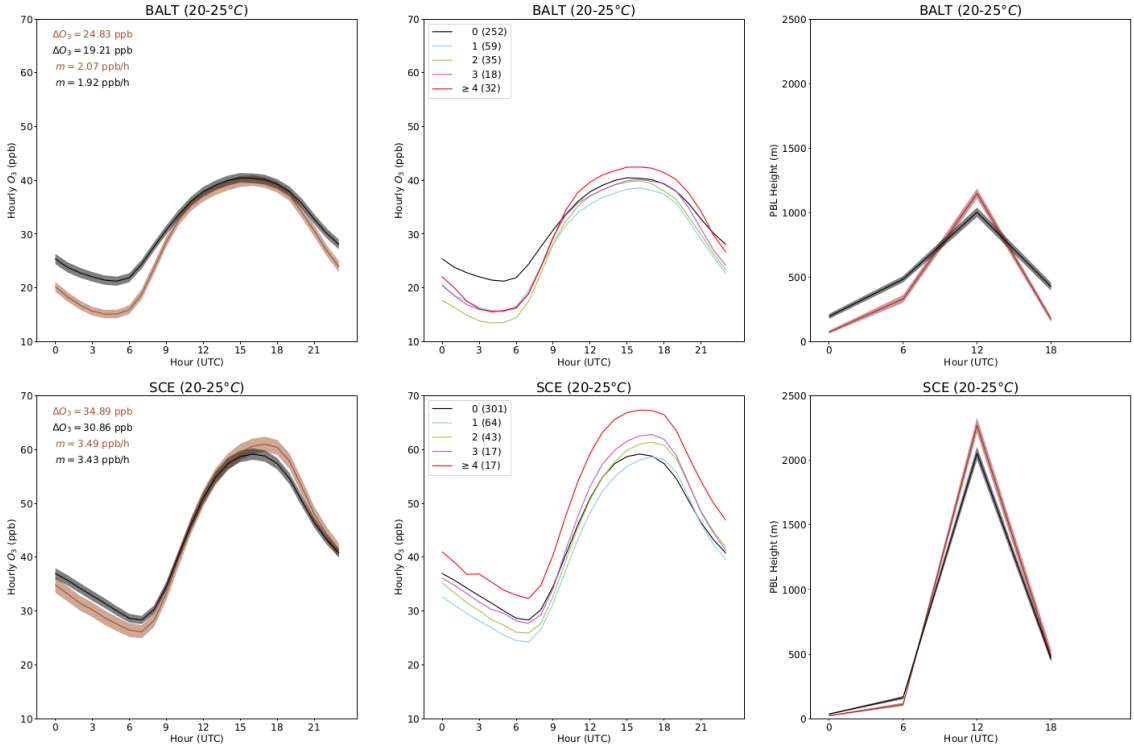

Figure 6. Composites of the diurnal cycles of hourly O_3 and PBL height at two representative locations in BALT and SCE on stagnant and non-stagnant days with T_{max} within 20 – 25 °C. The times displayed on the x-axes are UTC while summer local time is UTC+3 for BALT and UTC+2 for SCE. Left panels: Average diurnal ozone profiles for the summer (JJA) 1998 – 2015 days with (brown) and without (black line) stagnation in BALT (top) and SCE (bottom). Shadings cover the 95% confidence interval. The amplitudes and increase rates of the stagnant (brown) and non-stagnant (black) diurnal cycles are displayed as ΔO_3 and *m* on the upper-left corners of the panels. Middle panels: Average diurnal ozone profiles for summer days based on the persistence of stagnation in BALT (top) and SCE (bottom). The black line represents non-stagnation, while the blue, green, purple and red lines represent one, two, three and four or more consecutive days with stagnation, respectively. The numbers in brackets indicate the total number of days considered for each case. Right panels: Evolution of PBL height (using data at 0, 6, 12 and 18 UTC) at both locations for stagnant (brown) and non-stagnant (black) days.

The left panels of Figures 6, S5 and S6 illustrate the average diurnal cycles of the hourly O_3 mixing ratios at the selected locations in the 8 regions, considering stagnant (brown) and non-stagnant (black) days, with 95% uncertainty estimates. The confidence intervals have been calculated using standard t-statistics (von Storch and Zwiers, 1999). Generally, the diurnal amplitude is significantly larger on stagnant days, as it increases by 2.5 to 10 ppb in 6 out of 8 selected grid cells (see ΔO_3 values at the upper left corners of the panels). The only exceptions are the locations in BRIT and NSC, where the amplitude hardly changes. In the former location, the number of days with T_{max} within 20 – 25 °C is not high enough to draw solid conclusions (see Figure S5 a, b), whereas NSC is by far the cluster with the lowest sensitivity of MDA8 O_3 to stagnation (Table 1).

The differences between stagnant and non-stagnant O_3 diurnal cycles are often due to the above-average daytime increase and/or nighttime decrease of O_3 during stagnant days, again with the exception of BRIT and NSC. The low nighttime ozone mixing ratios on stagnant days may be caused by enhanced chemical destruction and dry deposition under a stable nocturnal PBL. Indeed, the right panels of Figures 6, S5 and S6 prove that the average PBL height at 6 UTC is often lower than usual during stagnant nights. That is particularly the case for the locations with the strongest ozone decrease under stagnant conditions at that time of the day (grid cells in BALT, NCE, WE and EE). This results in a reduced O_3 baseline at the beginning of the day for these four locations and, to a lesser extent, for those in SCE and BRIT, while no clear effect is found for the grid cells in NSC and IBE. Thus we have shown that at most locations the occurrence of stagnation leads to below-average early morning PBL height and ozone on the same day.

By contrast, the stronger build-up of daytime ozone on stagnant days could be related to the accumulation of primary pollutants and subsequent photochemical production as well as to enhanced subsidence and accumulation of ozone under the stable anticyclonic conditions that characterize those days. The afternoon ozone maxima tend to be higher than average on stagnant days for the central/southern locations, in particular for the grid cells in WE and EE, and to lesser extent for those in IBE and SCE. The most noticeable effect of stagnation on daytime ozone for the grid cell in SCE is the shift of the highest mixing ratios to later hours in the evening, consistent with a synchronous shift in temperature under stagnant conditions at the same location (not shown). The average afternoon ozone maxima are also higher on stagnant than on non-stagnant days for the grid cell in NCE, while there is no clear impact or even a decrease for the other northern locations in BALT, BRIT and NSC. This is consistent with the unclear impact of stagnation on the MDA8 O_3 - temperature relationship (Figure 3, a, c, d) and the effect of southerly advection during non-stagnant days (Figure 5, a, c, d) shown previously for those regions.

We have also computed the daily ozone increase rate (defined as the daily amplitude divided by the period of time between the maximum and the minimum O_3 mixing ratios) at each location under stagnant and non-stagnant days. These values are displayed as *m* at the upper left corners of the left panels in Figures 6, S5 and S6. This rate changes from 2.0–2.6 ppb h^{-1} under non-stagnant conditions to 2.2–3.4 ppb h^{-1} during stagnant days at three of the central/southern locations, IBE, WE and EE (Figure S6). The largest increases of this rate are found for WE and EE (above 0.7 ppb h^{-1}). However, the increase at the grid cell in SCE is negligible (below 0.1 ppb h^{-1}), because of the mentioned late afternoon ozone maxima at this location under stagnant conditions. The daily ozone increase rate also rises at most of the northern locations under stagnant conditions, but the typical values are lower than those shown above, ranging from 0.9 ppb h^{-1} in NSC to 2.0–2.3 ppb h^{-1} in BRIT. These results suggest higher photochemical production in the

central/southern than in the northern locations, in line with expectations, as well as an enhancement of photochemical activity during stagnant days. Nevertheless, some of the processes previously mentioned (e.g. decrease of the early morning ozone baseline followed by enhanced vertical mixing and subsidence at daytime on stagnant days, southerly advection to northern regions under non-stagnant conditions) may be relevant to explain these differences.

Previous studies have considered four or more consecutive days with air stagnation at a given location as an air stagnation episode (Wang and Angell, 1999; Huang et al., 2017). Such episodes are not common in northern Europe (Garrido-Perez et al., 2018), but it is still possible to examine changes in the diurnal evolution of ozone during successive stagnation days. The middle panels of Figures 6, S5 and S6 display composites of O_3 diurnal cycles for non-stagnant days (black) as well as for one (blue), two (green), three (purple) and four or more (red) consecutive days with stagnation. Despite some limitations due to the small number of consecutive stagnant days at some locations, especially the grid cell in BRIT, the figures indicate that daytime ozone mixing ratios tend to increase with the persistence of air stagnation. The only exceptions are that location in BRIT and the one selected in NSC. Our results are in the same line as previous analyses which found the number of successive stagnation days as a good indicator of the build-up of MDA8 O_3 in most regions of the US (Sun et al., 2017). In addition, a number of studies have related the persistence of air stagnation or the associated stable anticyclonic conditions to the build-up of summer daily O_3 maximum and MDA8 O_3 in some regions of Europe (Ordóñez et al., 2005, 2017; Garrido-Perez, 2018). This also seems to be consistent with the well-known persistence of elevated MDA8 O_3 in Europe (e.g. Otero et al., 2016). However, this increase does not necessarily apply to the whole diurnal cycle. In fact, the first days with stagnation consistently show a lower daily O_3 minimum than non-stagnant days, but this minimum gradually increases with the persistence of stagnation, as found during daylight hours, again with the exception of BRIT and NSC. If air stagnation persists long enough, the early morning O_3 baseline can recover and even exceed the typical levels found during non-stagnant days at the locations in SCE and IBE. BALT, NCE, WE and EE present a similar build-up, but the early morning O_3 baseline during the most persistent stagnation episodes remains below that of non-stagnant days. Hence, it appears that the nighttime destruction of O_3 is enhanced under the shallow PBL during the first stagnant days at most locations and that this destruction is at least partially compensated by the accumulation of O_3 when consecutive days with stagnation occur. The increase in the early morning baseline at some locations, together with mixing of boundary layer air with ozone-rich air from the residual layer after sunrise as well as daytime photochemical production, will favor the occurrence of elevated MDA8 O_3 in the afternoon.

5. Discussion and conclusions

Climate change is expected to increase the risk of extreme air pollution events in the future. Southern Europe has been identified as a climate change hot spot (Diffenbaugh and Giorgi, 2012; de Sherbinin, 2014) and is projected to have multiple impacts. Among them, climate models have projected strong increases in temperature (Giorgi and Lionello, 2008; Barkhordarian et al., 2012) and atmospheric stagnation (Horton et al., 2012, 2014) in this region. Both phenomena are closely linked to elevated ozone concentrations and thus their exacerbation should make it harder to achieve air quality goals for this pollutant in the future. However, a recent study has questioned the relationship between summer air pollution and stagnation (Kerr and Waugh, 2018).

Keeping in mind that daily maximum temperature is the meteorological variable that mostly controls the afternoon ozone concentrations, this study has investigated the added value of a simple air stagnation index (Horton et al, 2012) to understand summer ozone variability in Europe. Building on the regional classification of MDA8 O_3 by Carro-Calvo et al. (2017), we have evaluated the joint effect of temperature and stagnation on summer ozone in eight regions (BRIT, NCE, NSC, BALT, IBE, WE, SCE, EE), finding considerable heterogeneity across the continent. The main findings are as follows:

- MDA8 O_3 mixing ratios consistently increase over central/southern Europe (IBE, WE, SCE, EE) and, to a lesser extent, NCE under stagnant conditions, but this has not been found for some temperature bins in three of the northern regions (BRIT, NSC, BALT). Under non-stagnant conditions and T_{max} within 20–25 °C (typical temperatures of fair weather conditions that allow photochemical production in northern Europe), such regions are affected by southerly advection, which is a known mechanism for the occurrence of ozone extremes in the north of the continent (Carro-Calvo et al., 2017).

- The ozone diurnal cycle in the central/southern regions and NCE exhibits larger amplitudes than usual when stagnation occurs, with low nighttime and high daytime mixing ratios in most of these regions. Stagnant nights are associated with stable shallow PBL and, presumably, enhanced dry deposition and chemical destruction of ozone. After sunrise, with the development of the PBL, mixing with air from the residual layer, accumulation of ozone and precursors, and photochemical production seem to be the main mechanisms involved in the build-up of daytime ozone.

- Low nighttime ozone mixing ratios during stagnant days are also a feature of BALT and BRIT, while afternoon ozone and consequently MDA8 O_3 are not clearly affected by stagnation. In particular, for the 20–25 °C temperature range considered here, afternoon ozone can even decrease under stagnant conditions in BRIT. However, these results should be interpreted with caution considering the limited number of occurrences observed and the fact that MDA8 O_3 in the same region increases on stagnant days for other temperature ranges.

- NSC is the region with the weakest sensitivity of ozone to stagnation. This is firstly evidenced from the poor correlation between the daily time series of average MDA8 O_3 and the percentage of stagnant area in the region (R=0.06). Moreover, the occurrence of stagnation hardly affects the ozone diurnal cycles for T_{max} within 20–25 °C and even yields decreases in the MDA8 O_3 mixing ratios for T_{max} above ~20 °C. Nonetheless, we note the results for this region are based on relative fewer surface ozone observations as compared to those in central/southern regions (i.e. less than 30 sites north of 62.5° N).

In short, we have been able to identify regions with different responses of summer ozone to the occurrence of air stagnation. It is remarkable that some of the central/southern European regions where stagnation has a clear impact on ozone have already undergone significant upward trends in stagnation over the last decades (Garrido-Perez et al., 2018) and are also likely to experience increases in the future (Horton et al., 2014). On the other hand, stagnation seems to exert a minor control on summer ozone over most of northern Europe. Consequently, observations of air stagnation occurrence and projections of increases in air stagnation should not directly be translated into enhanced summer ozone pollution if the sensitivity of this pollutant to stagnation has not been proved for a particular region.

Another relevant result of this paper is that the occurrence of air stagnation amplifies the diurnal cycles of summer ozone over some regions. While simulations of surface ozone by Chemical Transport Models (CTMs) are often evaluated against observations of MDA8 O_3 or other relevant cumulative metrics (e.g. Lupaşcu and Butler, 2019), understanding the differences in the performance of a set of model simulations for such metrics would require assessing the skill to reproduce the diurnal cycle of ozone. In fact, current global and regional CTMs present limitations at night and under stable conditions, partly because of the difficulty in resolving the stratified conditions near the surface and the depletion of ozone through surface deposition (Travis and Jacob, 2019, and references therein). Nighttime PBL dynamics and chemistry are crucial because they will determine the early morning ozone baseline and also influence morning radical chemistry, with important implications for the formation of daytime ozone (e.g. Brown and Stutz, 2012). On the other hand, following the development of the PBL at daytime, the entrainment of ozone-rich air from the upper levels to the ground has been proved to be an important transport mechanism of summer ozone smog (e.g. Hu et al., 2018, and references therein). Therefore, special attention should be given to quantifying the contribution of individual processes such us horizontal and vertical advection, vertical diffusion, dry deposition and chemistry to the ozone budget under different meteorological conditions. This can be achieved through the use of probing techniques like Integrated Process Rate analysis (IPR), which provides detailed mass balance information for the aforementioned processes in some regional CTMs (e.g. Liu et al., 2007; Gonçalves et al., 2009; Lyu et al., 2019). Our findings about the differing impacts of air stagnation on the ozone diurnal cycles across Europe provide good observational constrains for the evaluation of such processes under stagnant vs. non-stagnant conditions. Furthermore, periods of persistent stagnant situations can be very appropriate to test the ability of CTMs to reproduce PBL dynamics and the evolution of ozone concentrations.

Acknowledgments

JMGP was supported by a predoctoral research grant awarded by the Spanish Ministerio de Educación, Cultura y Deporte (FPU16/01972) and CO by the Ramón y Cajal Programme of the Spanish Ministerio de Economía y Competitividad [grant number RYC-2014-15036]. JLS was funded by the Ubben Program for Climate and Carbon Science. We also acknowledge support from STEADY (CGL2017-83198-R), project funded by the Spanish Ministerio de Economía, Industria y Competitividad. ERA-Interim reanalysis was provided by ECMWF. We are grateful to Leopoldo Carro-Calvo for providing the regionalization of the gridded ozone dataset. The authors thank three anonymous reviewers for their useful comments.

References

Ashmore, M.R., 2005. Assessing the future global impacts of ozone on vegetation. Plant, Cell Environ. 28, 949–964. https://doi.org/10.1111/j.1365-3040.2005.01341.x

Barkhordarian, A., Bhend, J., von Storch, H., 2012. Consistency of observed near surface temperature trends with climate change projections over the Mediterranean region. Clim. Dyn. 38, 1695–1702. https://doi.org/10.1007/s00382-011-1060-y

Bloomer, B.J., Stehr, J.W., Piety, C.A., Salawitch, R.J., Dickerson, R.R., 2009, Observed relationships of ozone air pollution with temperature and emissions. Geophys. Res. Lett. 36, L09803. https://doi.org/10.1029/2009GL037308

Bloomfield, P., Royle, J.A., Steinberg, L.J., Yang, Q., 1996. Accounting for meteorological effects in measuring urban ozone levels and trends. Atmos. Environ. 30, 3067–3077. https://doi.org/10.1016/1352-2310(95)00347-9

Brown, S.S., Stutz, J., 2012. Nighttime radical observations and chemistry. Chem. Soc. Rev. 41, 6405–6447. https://doi.org/10.1039/c2cs35181a

Carro-Calvo, L., Ordóñez, C., García-Herrera, R., Schnell, J.L., 2017. Spatial clustering and meteorological drivers of summer ozone in Europe. Atmos. Environ. 167, 496–510. https://doi.org/10.1016/j.atmosenv.2017.08.050

Dawson, J.P., Bloomer, B.J., Winner, D.A., Weaver, C.P., 2014. Understanding the meteorological drivers of U.S. particulate matter concentrations in a changing climate. Bull. Am. Meteorol. Soc. 95, 521–532. https://doi.org/10.1175/BAMS-D-12-00181.1

de Sherbinin, A., 2014. Climate change hotspots mapping: What have we learned? Clim. Change 123, 23–37. https://doi.org/10.1007/s10584-013-0900-7

Dee, D.P., Uppala, S.M., Simmons, A.J., Berrisford, P., Poli, P., Kobayashi, S., Andrae, U., Balmaseda, M.A., Balsamo, G., Bauer, P., Bechtold, P., Beljaars, A.C.M., van de Berg, L., Bidlot, J., Bormann, N., Delsol, C., Dragani, R., Fuentes, M., Geer, A.J., Haimberger, L., Healy, S.B., Hersbach, H., Hólm, E. V., Isaksen, L., Kållberg, P., Köhler, M., Matricardi, M., Mcnally, A.P., Monge-Sanz, B.M., Morcrette, J.J., Park, B.K., Peubey, C., de Rosnay, P., Tavolato, C., Thépaut, J.N., Vitart, F., 2011. The ERA-Interim reanalysis: Configuration and performance of the data assimilation system. Q. J. R. Meteorol. Soc. 137, 553–597. https://doi.org/10.1002/qj.828

Diffenbaugh, N.S., Giorgi, F., 2012. Climate change hotspots in the CMIP5 global climate model ensemble. Clim. Change 114, 813–822. https://doi.org/10.1007/s10584-012-0570-x

Fehsenfeld, F., Calvert, J., Fall, R., Goldan, P., Guenther, A.B., Hewitt, C.N., Lamb, B., Trainer, M., Westberg, H., Zimmerman, P., 1992. Emissions of volatile organic compounds from vegetation and the implications for atmospheric chemistry. Global Biogeochem. Cycles 6, 389–430. https://doi.org/10.1029/92GB02125

Fiore, A.M., Naik, V., Leibensperger, E.M., 2015. Air quality and climate connections. J. Air Waste Manag. Assoc. 65, 645–685. https://doi.org/10.1080/10962247.2015.1040526

Garrido-Perez, J.M., Ordóñez, C., García-Herrera, R., Barriopedro, D., 2018. Air stagnation in Europe: Spatiotemporal variability and impact on air quality. Sci. Total Environ. 645, 1238–1252. https://doi.org/10.1016/j.scitotenv.2018.07.238

Giorgi, F., Lionello, P., 2008. Climate change projections for the Mediterranean region. Glob. Planet. Change 63, 90–104. https://doi.org/10.1016/j.gloplacha.2007.09.005

Gonçalves, M., Jiménez-Guerrero, P., Baldasano, J.M., 2009. Contribution of atmospheric processes affecting the dynamics of air pollution in South-Western Europe during a typical summertime photochemical episode. Atmos. Chem. Phys. 9, 849–864. https://doi.org/10.5194/acp-9-849-2009

Horton, D.E., Harshvardhan, Diffenbaugh, N.S., 2012. Response of air stagnation frequency to anthropogenically enhanced radiative forcing. Environ. Res. Lett. 7, 044034. https://doi.org/10.1088/1748-9326/7/4/044034

Horton, D.E., Skinner, C.B., Singh, D., Diffenbaugh, N.S., 2014. Occurrence and persistence of future atmospheric stagnation events. Nat. Clim. Chang. 4, 698–703. https://doi.org/10.1038/nclimate2272

Hu, J., Emile-Geay, J., Partin, J., 2017. Correlation-based interpretations of paleoclimate data – where statistics meet past climates. Earth Planet. Sci. Lett. 459, 362-371. https://doi.org/10.1016/j.epsl.2016.11.048

Hu, J., Li, Y., Zhao, T., Liu, J., Hu, X.M., Liu, D., Jiang, Y., Xu, J., Chang, L., 2018. An important mechanism of regional O_3 transport for summer smog over the Yangtze River Delta in eastern China. Atmos. Chem. Phys. 18, 16239–16251. https://doi.org/10.5194/acp-18-16239-2018

Huang, Q., Cai, X., Song, Y., Zhu, T., 2017. Air stagnation in China (1985 – 2014): climatological mean features and trends. Atmos. Chem. Phys. 17, 7793–7805. https://doi.org/10.5194/acp-17-7793-2017

Huang, Q., Cai, X., Wang, J., Song, Y., Zhu, T., 2018. Climatological study of the Boundary-layer air Stagnation Index for China and its relationship with air pollution. Atmos. Chem. Phys. 18, 7573–7593. https://doi.org/10.5194/acp-18-7573-2018

Jacob, D.J., Winner, D.A., 2009. Effect of climate change on air quality. Atmos. Environ. 43, 51–63. https://doi.org/10.1016/j.atmosenv.2008.09.051

Kerr, G.H., Waugh, D.W., 2018. Connections between summer air pollution and stagnation. Environ. Res. Lett. 13, 084001. https://doi.org/10.1088/1748-9326/aad2e2

Kuebler, J., Van Den Bergh, H., Russell, A.G., 2001. Long-term trends of primary and secondary pollutant concentrations in Switzerland and their response to emission controls and economic changes. Atmos. Environ. 35, 1351–1363. https://doi.org/10.1016/S1352-2310(00)00401-5

Leibensperger, E.M., Mickley, L.J., Jacob, D.J., 2008. Sensitivity of US air quality to mid-latitude cyclone frequency and implications of 1980–2006 climate change. Atmos. Chem. Phys. 8, 7075–7086. https://doi.org/10.5194/acp-8-7075-2008

Liu, L., Andreani-Aksoyoglu, S., Keller, J., Ordóñez, C., Junkermann, W., Hak, C., Braathen, G.O., Reimann, S., Astorga-Llorens, C., Schultz, M., Prévôt, A.S.H., Isaksen, I.S.A., 2007. A photochemical modeling study of ozone and formaldehyde generation and budget in the Po basin. J. Geophys. Res. Atmos. 112, D22303. https://doi.org/10.1029/2006JD008172

Lupaşcu, A., Butler, T., 2019. Source attribution of European surface O_3 using a tagged O_3 mechanism. Atmos. Chem. Phys. Discuss. https://doi.org/10.5194/acp-2019-225

Lyu, X., Wang, N., Guo, H., Xue, L., Jiang, F., Zeren, Y., Cheng, H., Cai, Z., Han, L., Zhou, Y., 2018. Causes of a continuous summertime O_3 pollution event in Jinan, a central city in the North China Plain. Atmos. Chem. Phys. 19, 3025–3042. https://doi.org/10.5194/acp-19-3025-2019

Meehl, G.A., Tebaldi, C., Tilmes, S., Lamarque, J.F., Bates, S., Pendergrass, A., Lombardozzi, D., 2018. Future heat waves and surface ozone. Environ. Res. Lett. 13, 064004. https://doi.org/10.1088/1748-9326/aabcdc

Ordóñez, C., Barriopedro, D., García-Herrera, R., Sousa, P.M., Schnell, J.L., 2017. Regional responses of surface ozone in Europe to the location of high-latitude

blocks and subtropical ridges. Atmos. Chem. Phys. 17, 3111–3131. https://doi.org/10.5194/acp-17-3111-2017

Ordóñez, C., Mathis, H., Furger, M., Henne, S., Hüglin, C., Staehelin, J., Prévôt, A.S.H., 2005. Changes of daily surface ozone maxima in Switzerland in all seasons from 1992 to 2002 and discussion of summer 2003. Atmos. Chem. Phys. 5, 1187–1203. https://doi.org/10.5194/acp-5-1187-2005

Orlando, J.J., Tyndall, G.S., Calvert, J.G., 1992. Thermal decomposition pathways for peroxyacetyl nitrate (PAN): Implications for atmospheric methyl nitrate levels. Atmos. Environ. Part A, Gen. Top. 26, 3111–3118. https://doi.org/10.1016/0960-1686(92)90468-Z

Otero, N., Sillmann, J., Mar, K.A., Rust, H.W., Solberg, S., Andersson, C., Engardt, M., Bergström, R., Bessagnet, B., Colette, A., Couvidat, F., Cuvelier, C., Tsyro, S., Fagerli, H., Schaap, M., Manders, A., Mircea, M., Briganti, G., Cappelletti, A., Adani, M., D'Isidoro, M., Pay, M.T., Theobald, M., Vivanco, M.G., Wind, P., Ojha, N., Raffort, V., Butler, T., 2018. A multi-model comparison of meteorological drivers of surface ozone over Europe. Atmos. Chem. Phys. 18, 12269–12288. https://doi.org/10.5194/acp-18-12269-2018

Otero, N., Sillmann, J., Schnell, J.L., Rust, H.W., Butler, T., 2016. Synoptic and meteorological drivers of extreme ozone concentrations over Europe. Environ. Res. Lett 11, 024005. https://doi.org/10.1088/1748-9326/11/2/024005

Petetin, H., Thouret, V., Athier, G., Blot, R., Boulanger, D., Cousin, J.-M., Gaudel, A., Nédélec, P., Cooper, O., 2016. Diurnal cycle of ozone throughout the troposphere over Frankfurt as measured by MOZAIC-IAGOS commercial aircraft. Elem. Sci. Anthr. 4, 000129. https://doi.org/10.12952/journal.elementa.000129

Porter, W.C., Heald, C.L., 2019. The mechanisms and meteorological drivers of the ozone-temperature relationship. Atmos. Chem. Phys. Discuss. https://doi.org/10.5194/acp-2019-140

Pyrgou, A., Hadjinicolaou, H., Santamouris, M., 2018. Enhanced near-surface ozone under heatwave conditions in a Mediterranean island. Sci. Rep. 8, 9191. https://doi.org/10.1038/s41598-018-27590-z

REVIHAAP, 2013. Review of evidence on health aspects of air pollution - REVIHAAP Project. Technical Report. World Health Organization Regional Office for Europe. Bonn. Available at: http://www.euro.who.int/__data/assets/pdf_file/0004/193108/REVIHAAP-Final-technical-report-final-version.pdf.

Schnell, J.L., Holmes, C.D., Jangam, A., Prather, M.J., 2014. Skill in forecasting extreme ozone pollution episodes with a global atmospheric chemistry model. Atmos. Chem. Phys. 14, 7721–7739. https://doi.org/10.5194/acp-14-7721-2014

Schnell, J.L., Prather, M.J., 2017. Co-occurrence of extremes in surface ozone, particulate matter, and temperature over eastern North America. Proc. Natl. Acad. Sci. 114, 2854–2859. https://doi.org/10.1073/pnas.1614453114

Schnell, J.L., Prather, M.J., Josse, B., Naik, V., Horowitz, L.W., Cameron-Smith, P., Bergmann, D., Zeng, G., Plummer, D.A., Sudo, K., Nagashima, T., Shindell, D.T., Faluvegi, G., Strode, S.A., 2015. Use of North American and European air quality

networks to evaluate global chemistry-climate modeling of surface ozone. Atmos. Chem. Phys. 15, 10581–10596. https://doi.org/10.5194/acp-15-10581-2015

Shen, L., Mickley, L.J., Gilleland, E., 2016. Impact of increasing heat waves on U.S. ozone episodes in the 2050s: Results from a multimodel analysis using extreme value theory. Geophys. Res. Lett. 43, 4017–4025. https://doi.org/10.1002/ 2016GL068432

Simpson, D., 1995. Biogenic emissions in Europe: 2. Implications for ozone control strategies. J. Geophys. Res. 100, 22891–22906. https://doi.org/10.1029/95jd01878

Steiner, A.L., Davis, A.J., Sillman, S., Owen, R.C., Michalak, A.M., Fiore, A.M., 2010. Observed suppression of ozone formation at extremely high temperatures due to chemical and biophysical feedbacks. Proc. Natl Acad. Sci. 107, 19685–90. https://doi.org/ 10.1073/pnas.1008336107

Sun, W., Hess, P., Liu, C., 2017. The impact of meteorological persistence on the distribution and extremes of ozone. Geophys. Res. Lett. 44, 1545–1553. https://doi.org/10.1002/2016GL071731

Tai, A.P.K., Martin, M.V., Heald, C.L., 2014. Threat to future global food security from climate change and ozone air pollution. Nat. Clim. Chang. 4, 817–821. https://doi.org/10.1038/nclimate2317

Tarasova, O.A., Karpetchko, A.Y., 2003. Accounting for local meteorological effects in the ozone time-series of Lovozero (Kola Peninsula). Atmos. Chem. Phys. 3, 941–949. https://doi.org/10.5194/acp-3-941-2003

Tørseth, K., Aas, W., Breivik, K., Fjeraa, A.M., Fiebig, M., Hjellbrekke, A.G., Lund Myhre, C., Solberg, S., Yttri, K.E., 2012. Introduction to the European Monitoring and Evaluation Programme (EMEP) and observed atmospheric composition change during 1972-2009. Atmos. Chem. Phys. 12, 5447–5481. https://doi.org/10.5194/acp-12-5447-2012

Travis, K.R., Jacob, D.J., 2019. Systematic bias in evaluating chemical transport models with maximum daily 8 h average (MDA8) surface ozone for air quality applications: a case study with GEOS-Chem v9.02. Geosci. Model Dev. https://doi.org/10.5194/gmd-12-3641-2019

Vautard, R., Honoré, C., Beekmann, M., Rouil, L., 2005. Simulation of ozone during the August 2003 heat wave and emission control scenarios. Atmos. Environ. 39, 2957–2967. https://doi.org/10.1016/j.atmosenv.2005.01.039

von Storch, H., Zwiers, F.W., 1999. Statistical analysis in climate research, Cambridge University Press, Cambridge, UK. https://doi.org/10.1017/CBO9780511612336

Wang, J.X.L., Angell, J.K., 1999. Air Stagnation Climatology for the United States. NOAA/Air Resour. Lab. ATLAS 1.

Wang, X., Dickinson, R.R.E., Su, L., Zhou, C., Wang, K., 2018. $PM_{2.5}$ pollution in China and how it has been exacerbated by terrain and meteorological conditions. Bull. Am. Meteorol. Soc. 99, 105–120. https://doi.org/10.1175/BAMS-D-16-0301.1

Wang, X., Wang, K., Su, L., 2016. Contribution of atmospheric diffusion conditions to the recent improvement in air quality in China. Sci. Rep. 6, 36404. https://doi.org/10.1038/srep36404

739 Wesely, M.L., 1989. Parametrization of surface resistances to gaseous dry
740 deposition in regional-scale numerical models. Atmos. Environ. 23, 1293–1304.
741 https://doi.org/10.1016/0004-6981(89)90153-4

742 Wilks, D. S.: Statistical Methods in the Atmospheric Sciences, 3rd Edition,
743 Academic Press, Oxford, UK, 2011.

744 Xu, D., Yap, D., Taylor, P.A., 1996. Meteorologically adjusted ground level ozone
745 trends in Ontario. Atmos. Environ. 30, 1117–1124. https://doi.org/10.1016/1352-
746 2310(95)00331-2